Quantum pBac: An effective, high-capacity *piggyBac*-based gene integration vector system for unlocking gene therapy potential

Wei-Kai Hua[1,*], Jeff C. Hsu[1,*], Yi-Chun Chen[1,*], Peter S. Chang[1], Kuo-Lan Karen Wen[1], Po-Nan Wang[2], Yi-Shan Yu[1], Ying-Chun Chen[1], I-Cheng Cheng[1], Sareina Chiung-Yuan Wu[1,†]

[1]GenomeFrontier Therapeutics, Inc. Taipei City, Taiwan (R.O.C.)

[2]Division of Hematology, Chang Gung Medical Foundation, Linkou Branch, Taipei City, Taiwan (R.O.C.)

[*] These authors contributed equally to this work and should be considered joint first author. Their authorship order is interchangeable

[†]Correspondence should be addressed to:

S.C.-Y.W. (sareina@genomefrontier.com) 23F, Bldg. C, No. 95, Sec. 1, Xintai 5th Rd., Xizhi Dist., New Taipei City 221416; +886-2-26558766;

This work was performed in Taipei City, Taiwan (R.O.C.)

Short title: *Quantum pBac* for unlocking gene therapy potential

Abstract

Recent advances in gene therapy have brought novel treatment options for cancer. However, the full potential of this approach has yet to be unlocked due to the safety concerns and limited payload capacity of commonly utilized viral vectors. Virus-free DNA transposons, including *piggyBac*, have potential to obviate these shortcomings. In this study, we improved a previously developed modified *piggyBac* system with superior transposition efficiency. We demonstrated that the internal domain sequences (IDS) within the 3' terminal repeat domain of hyperactive *piggyBac* (*hyPB*) donor vector contain dominant enhancer elements. Plasmid-free donor vector devoid of IDS was used in conjunction with a helper plasmid expressing *Quantum PBase*™ v2 to generate an optimal *piggyBac* system, *Quantum pBac*™ (*qPB*), for use in T cells. Cells transfected with *qPB* expressing CD20/CD19 CAR outperformed those transfected with the same donor vector and plasmid expressing *hyPB* transposase in terms of CAR-T cell production. Importantly, *qPB* yielded mainly $CD8^+$ CAR-T_{SCM} cells, and the *qPB*-induced CAR-T cells effectively eliminated CD20/CD19-expressing tumor cells both *in vitro* and *in vivo*. Our findings confirm *qPB* as a promising virus-free vector system with a payload capacity to incorporate multiple genes. This system is highly efficient and potentially safe for mediating transgene integration.

Introduction

Gene therapy often requires stable, long-term expression of therapeutic transgene(s) in cells. Such prolonged expression can be accomplished by engineering cells either *ex vivo* or *in vivo* using viral or non-viral vector systems. Viral vectors are most commonly used for gene therapy due to their high efficiencies of gene delivery and integration, which confer stable and long-term gene expression. However, viral vectors have several intrinsic limitations, including: (1) limited payload capacity that severely restricts the repertoire of genes that can be integrated[1]; (2) genotoxicity arising from preferential integration into sites near or within active gene loci that may negatively impact the expression and/or function(s) of genes[2–7]; (3) a cellular proclivity for silencing genes introduced by viral vectors, presumably due to cellular immunity[8,9]; and (4) safety concerns related to immunogenicity of viral vectors[10]. Additionally, production of viral vectors for clinical trials is costly, time-consuming (> 6 months), and supply-constrained, presenting significant obstacles to the routine use of viral vectors in medical practice[11].

In recent years, many advances have been made in non-viral gene delivery technologies, such as virus-free DNA transposons. These advancements may be capable of bypassing the shortcomings of viral vectors, and transposon technology has emerged as an especially promising vector system for gene therapy[12,13]. The great promise of transposon technology is largely due to its effective gene integration capability[14]. DNA transposons, also known as mobile elements or jumping genes, are genetic elements with the ability to transverse the genome

through a “cut-and-paste” mechanism. In nature, a simple DNA transposon contains a transposase gene flanked by terminal repeat sequences. During the transposition process, the ability of transposase to act on virtually any DNA sequence flanked by the terminal repeat sequences makes DNA transposons particularly attractive as vectors for gene therapy. To turn DNA transposons into tools for genetic engineering, researchers have developed controllable bi-component vector systems, consisting of (1) a helper plasmid expressing the transposase and (2) a donor plasmid with exogenous DNA of interest flanked by the transposon terminal repeat sequences. Currently, *Sleeping Beauty* and *piggyBac* are thought to be the most promising DNA transposons for human gene therapy and have been clinically explored as vectors for several CAR-T cell therapies. Unlike *Sleeping Beauty*, which was reconstructed from the salmon genome[15,16], *piggyBac* was derived from the cabbage looper moth *Trichoplusia ni* and is naturally active in humans[17–19]. By introducing amino acid mutations to the transposase, a hyperactive *piggyBac* (*hyPB*) transposase, (*hyPBase*) and two hyperactive transposases of *Sleeping Beauty* (SB100X and hyperactive SB100X, which is 30% more active than SB100X) were developed[20–24]. When an exogenous gene is delivered to primary human T cells *ex vivo*, *hyPBase* can increase transposition efficiency by 2- to 3-fold compared with *piggyBac* or SB100X transposases. Previously, we shortened the *piggyBac* terminal repeat domain (TRD) sequences and observed a 2.6-fold increase in transposition activity mediated by *piggyBac* in HEK293 cells[25]. We also demonstrated that the activity of *hyPBase* can be increased by another 2- to 3-fold by fusing the transposase

84 with various peptides[26]. In this study, we address whether the *piggyBac* system
85 can be further developed for therapeutic application, including increasing its cargo
86 capacity relative to those of currently available *piggyBac* systems. To do so, we
87 generated *Quantum pBac*™ (*qPB*), a binary *piggyBac* system comprising a
88 plasmid-free donor vector and a helper plasmid expressing the molecular-
89 engineered *hyPBase*, *Quantum PBase*™ (*qPBase*) *v2*. This simple, robust and
90 potentially safe vector system can be used to generate potent CD19/CD20 dual-
91 targeting CAR-T cells for treatment of B cell malignancies.
92

93 **Results**

94 **Micro-*piggyBac* possesses significantly lower enhancer activity compared**
95 **to mini-*piggyBac***

96 In the initial clinical trial of retrovirus-based gene therapy for SCID-X1, there
97 was evidence of malignancies caused by vector-mediated insertional activation of
98 proto-oncogenes. The currently available minimal *piggyBac* transposon vector,
99 designated as mini-*piggyBac* here, contains 5' (244 bp) and 3' (313 bp) TRD *cis*
100 elements, which are transposed along with gene of interest into the genome. Each
101 TRD contains a Terminal Inverted Repeat (TIR; also known as inverted minimal
102 terminal repeats) sequence and an internal domain sequence (IDS)[27]. To minimize
103 the potential risk of insertional mutagenesis caused by gene delivery vectors in
104 gene therapy, we had previously generated micro-*piggyBac*. This vector contains
105 the 5' (67 bp) and 3' (40 bp) TIR sequences of mini-*piggyBac*, but the respective
106 IDS are absent (Figure 1)[25]. Nevertheless, it remained unclear whether the TRDs

107 of mini-*piggyBac* and/or TIRs of micro-*piggyBac* harbor enhancer and/or silencer
108 activities. To address this issue, a panel of luciferase reporter constructs
109 containing individual TRD or TIR sequences was generated and examined in
110 insect Sf9 cells, human HEK293 cells, and human Jurkat T cells (Figure 1).

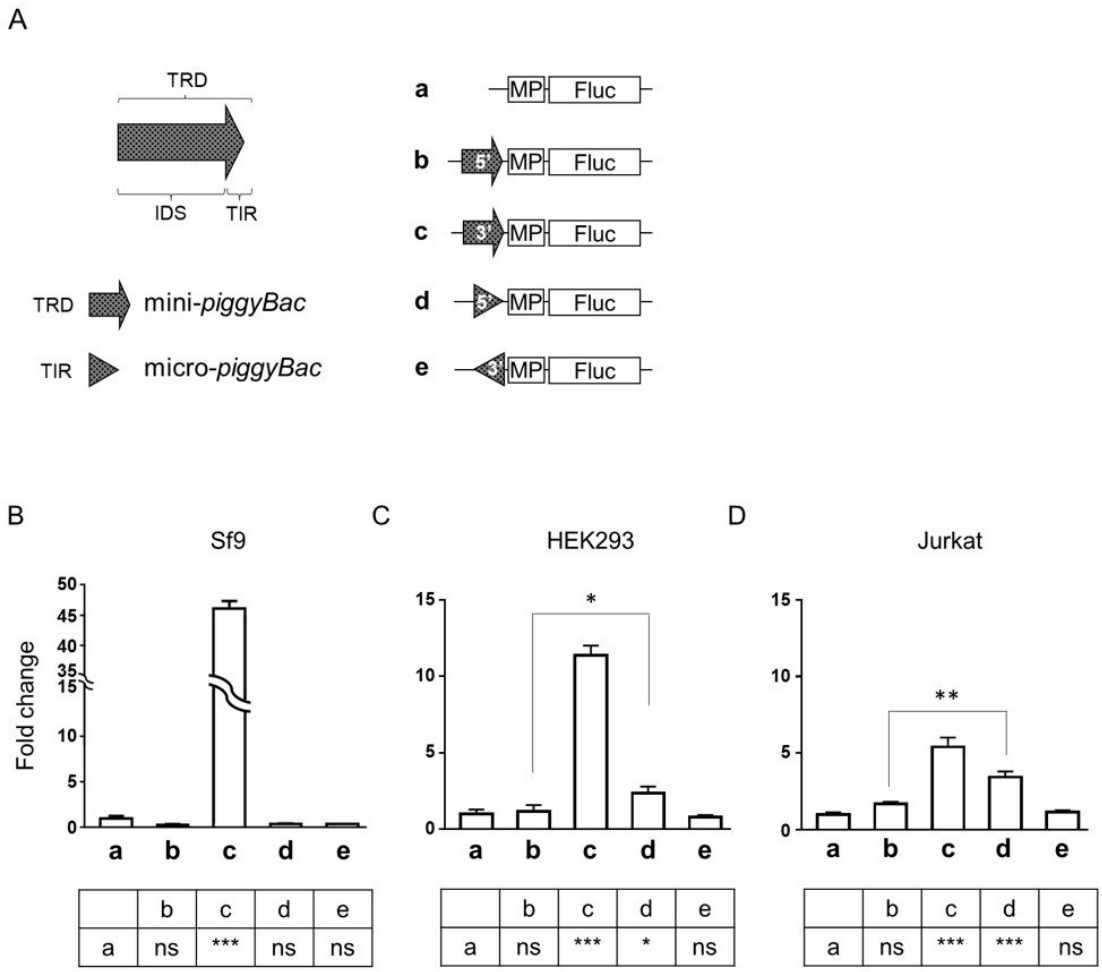

111

112 **Figure 1. Enhancer/silencer activity of mini-*piggyBac* TRDs and micro-*piggyBac* TIRs**
113 (A) Schematic depicts the panel of luciferase reporter constructs containing a CMV minimal
114 promoter (MP) and firefly luciferase (*Fluc*) gene, with or without the 5' or 3' TRDs from mini-
115 *piggyBac* or 5' or 3' TIRs from micro-*piggyBac* inserted upstream of MP. Luciferase activities
116 exhibited by the reporter constructs of (A) in (B) Sf9, (C) HEK293, and (D) Jurkat cells. Results are
117 shown as mean fold changes in luciferase activity ± standard deviation (SD; normalized first to

118 Renilla luciferase activity and then to the luciferase activity obtained from cells transfected with
119 construct a). Statistical analysis comparing luciferase activities obtained from cells transfected with
120 construct **a** and those from cells transfected with constructs **b**-**e** are summarized in the lower panels
121 (boxed regions). * $p < 0.05$, ** $p < 0.01$, *** $p < 0.001$. N = 3 (triplicate).
122

123 Compared to the control (Figure 1A, construct **a**), the 3' TRD of mini-
124 *piggyBac* (construct **c**) but not 3' TIR of micro-*piggyBac* (construct **e**) produced
125 significantly higher luciferase activity across all three cell types (Figure 1B-1D),
126 suggesting that enhancer activity is present in the 3' IDS of mini-*piggyBac*. On the
127 other hand, a slightly yet significantly enhanced luciferase activity was detected in
128 5' TIR of micro-*piggyBac* but not 5' TRD of mini-*piggyBac* in both HEK293 and
129 Jurkat cells. This result suggests the presence of a minimal level of enhanced
130 activity in the 5' TIR and/or silencer activity in the 5' IDS of TRD (Figure 1B-1D).
131 Taken together, the data suggest that micro-*piggyBac* possesses significantly
132 lower enhancer activity compared to mini-*piggyBac*.

133 **Shortening of donor vector backbone in combination with *Quantum PBase*™**
134 **(*qPBase*) *v2* enhances the transposition activity of micro-*piggyBac* in T cells**

135 The significantly reduced enhancer activity of TIRs suggested that micro-
136 *piggyBac* may be safer than mini-*piggyBac* for gene therapy applications. We
137 therefore focused on micro-*piggyBac* and determined whether its transposition
138 activity may be further enhanced by shortening the donor vector backbone (i.e.,
139 the sequences outside the TIR-spanning region). We constructed two donor
140 vectors named micro-*piggyBac*-Short and micro-*piggyBac*-Long. Both of these

141 vectors contain TIRs (micro) and either retains (Long) or is devoid of (Short)
142 replication components in its backbone, namely the replication origin and antibiotic
143 genes. A third donor vector, mini-*piggyBac* Long, which contains TRDs (mini) and
144 retains the replication components in its backbone (Long), was also constructed
145 for comparison; its combination with helper plasmid expressing *hyPBase*
146 (collectively called "hyperactive *piggyBac*" or "*hyPB*") is currently the most
147 advanced *piggyBac* system available (Figure 2A). We co-electroporated HEK293,
148 Jurkat or human primary T cells with different combinations of these donor vectors
149 and helper plasmids expressing wild-type *PBase* (pCMV-Myc-PBase), *hyPBase*
150 (pCMV-HA-hyPBase), and *qPBase v1* or *v2* (pCMV-qPBase_v1 and pCMV-

151 qPBase_v2, respectively). We then determined and compared the transposition

152 efficiencies of these donor vector and helper plasmid combinations (Figure 2A).

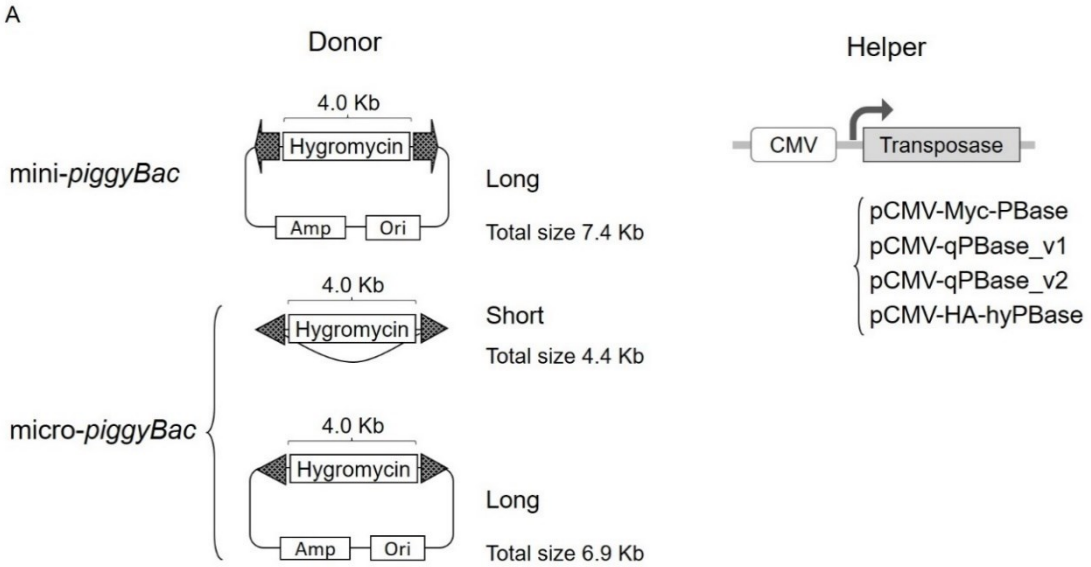

153

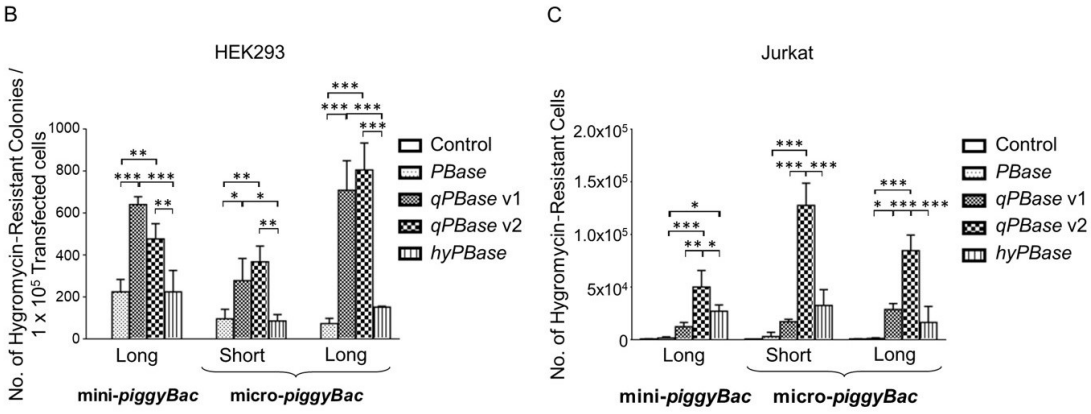

154

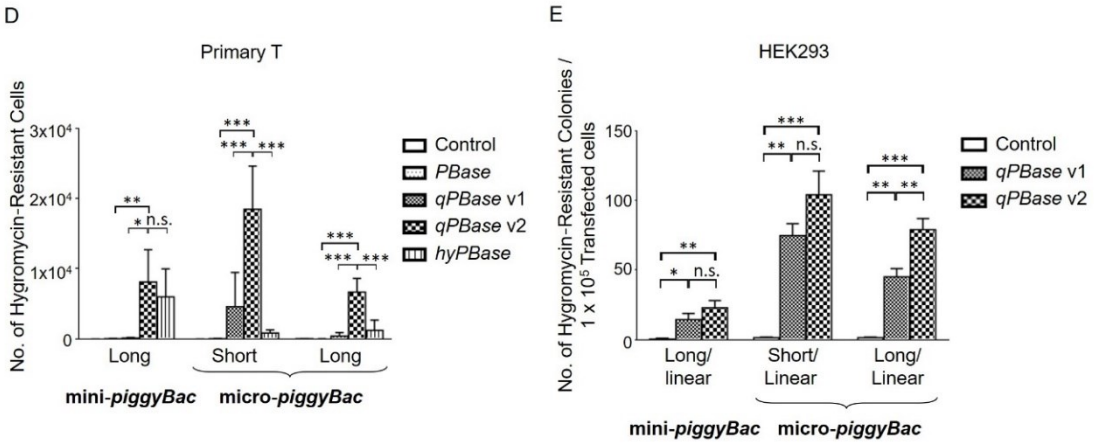

Figure 2. Transposition activities of various combinations of donor vectors and helper plasmids in human cells

(A) Schematic depicts the *piggyBac* system with various donor vectors and helper plasmids. Transposition activity of the indicated combination of donor vector and helper plasmid in (B) HEK293, (C) Jurkat, and (D) primary T cells. (E) Transposition activity of the indicated combination of linearized donor vector and helper plasmid in HEK293 cells. Results are shown as mean ± SD (B-E). n.s. not statistically significant, * $p < 0.05$, ** $p < 0.01$, *** $p < 0.001$. N = 3 (triplicate).

As shown, *hyPBase*, either in combination with mini-*piggyBac*-Long or micro-*piggyBac*-Short or -Long, markedly enhanced transposition compared to *PBase* in T cells but not in HEK293 cells. On the other hand, *qPBase* v1 markedly enhanced transposition compared to *hyPBase* in HEK293 cells but not in T cells (Figure 2B-2D). These results suggest that the transposition activity of *hyPBase* and *qPBase v1* are likely cell-type-dependent. We also found that *qPBase v2* mediated the highest transposition activity in nearly all of the tested combinations and cell types. Importantly, when *qPBase v2* is accompanied by micro-*piggyBac*-Short donor vector, its transposition activity is by far the highest in both Jurkat and

173 primary T cells, and this combination is clearly superior to the hyperactive
174 *piggyBac* system, *hyPBase* in combination with mini-*piggyBac*-Long (Figures 2C
175 and 2D).

176 **Micro-*piggyBac* is superior to mini-*piggyBac* for advancing adeno-*piggyBac***
177 **hybrid vector for gene therapy**

178 Even though *piggyBac* is capable of integrating sizable DNA (> 100 kb), its
179 genome engineering efficiency is restricted by the effectiveness of gene delivery
180 methods. Electroporation is a particularly effective virus-free gene delivery method
181 commonly used in gene therapy. However, its transfection efficiency is inversely
182 correlated with the size of DNA delivered, as cell damage may be caused by
183 introduction of larger transgenes. Thus, to alleviate electroporation-associated
184 restrictions imposed on the *piggyBac* system, an adenovirus-*piggyBac* hybrid
185 system (Ad-iPB7) was developed[28]. Since the adenovirus genome exists in a
186 linear form, we examined the transposition activity of linearized forms of mini-
187 *piggyBac*-Long, micro-*piggyBac*-Short and micro-*piggyBac*-Long along with either
188 *qPBase v1* or *qPBase v2*. As shown in Figure 2E, both micro-*piggyBac*-Short and
189 micro-*piggyBac*-Long were superior to mini-*piggyBac*-Long. Moreover, when
190 linearized micro-*piggyBac*-Long donor vector was combined with *qPBase v2*, a

191 significantly greater transposition efficiency was observed relative to that when
192 *qPBase v1* transposase was used (Figure 2E).

193 **Minicircle micro-*piggyBac* is significantly more active than its parental**
194 **counterpart in both Jurkat and primary T cells**

195 A minicircle DNA is a plasmid-free nucleic acid sequence that is normally
196 generated by an *in vivo* recombination process, which excises prokaryotic plasmid
197 components such as the antibiotic resistance gene and bacterial origin of
198 replication. Minicircle DNA constructs offer several advantages, including
199 enhancements in gene delivery efficiency and stable transgene expression. These
200 advantages may be attributed to the small vector size of minicircle DNA, the
201 absence of antibiotic resistance genes, and the lack of gene silencing induced by
202 bacterial backbone sequences required for plasmid replication. We demonstrated
203 that removal of backbone sequences outside the TIR-spanning regions via a
204 cloning procedure (which shortens the vector length) enhanced transposition
205 efficiency (Figure 2). Therefore, we next used the Mark Kay minicircle system to
206 generate a minicircle form of the donor vector (Q-tdTomato-IRES-hygro) from its
207 parental plasmid counterpart (pQ-tdTomato-IRES-hygro) (Figure 3A)[29]. We carried
208 out the same transposition assay as described for Figure 2 and determined

209 whether transposition of donor vector in the minicircle form into the T cell genome

210 would be more efficient than that of its parental plasmid counterpart.

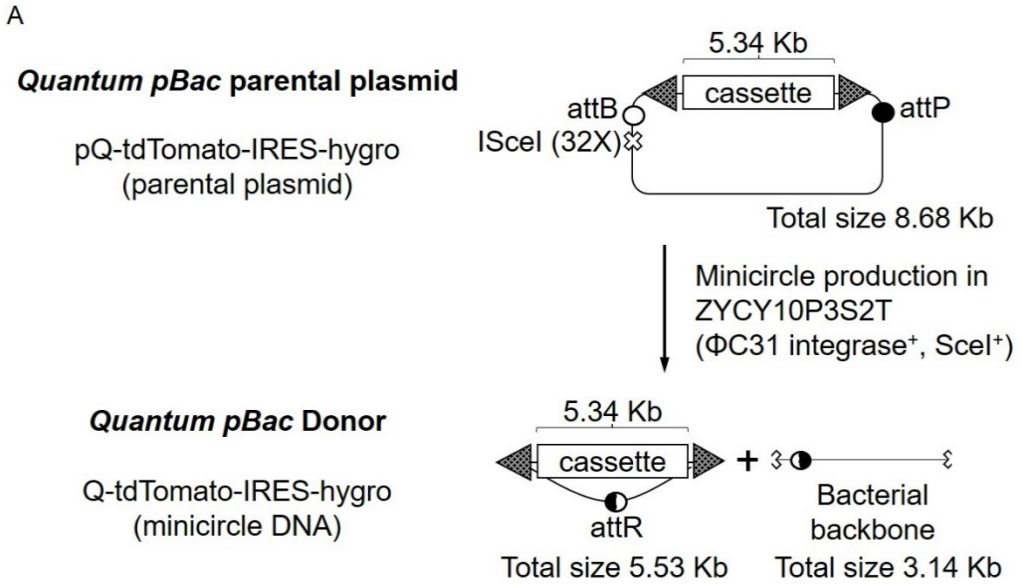

211

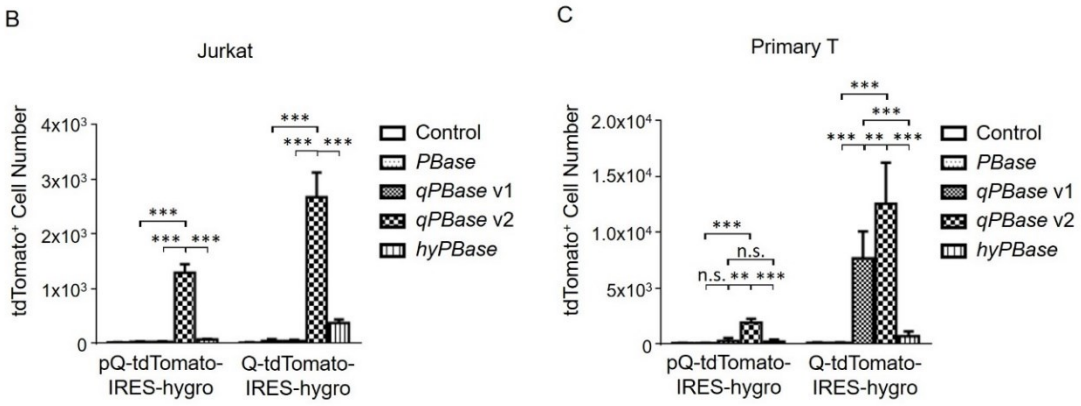

212

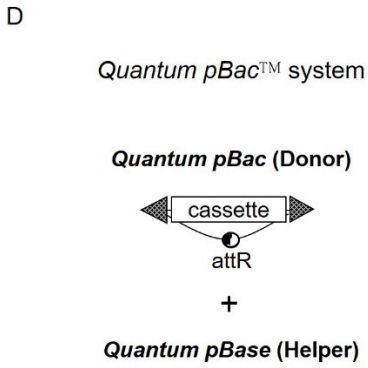

213

214 **Figure 3. Transposition activity of various transposases with donor vector in parental**
215 **plasmid or minicircle counterpart forms**
216 (A) Schematic depicts the generation of the *Quantum pBac*™ (*qPB*) donor vector. A gene cassette
217 carries *tdTomato* and *hygromycin* genes linked by IRES (Q-tdTomato-IRES-hygro) from the
218 parental plasmid (pQ-tdTomato-IRES-hygro). Transposition activities of the indicated combinations
219 of pQ-tdTomato-IRES-hygro or Q-tdTomato-IRES-hygro donor vectors and helper plasmids in (B)
220 Jurkat and (C) primary T cells. (D) Schematic depicts the two-component *qPB* system. Results are
221 shown as mean ± SD. n.s. not statistically significant, ** $p < 0.01$, *** $p < 0.001$. N = 3 (triplicate).
222

223 When donor vectors of parental plasmid (pQ-tdTomato-IRES-hygro) and
224 minicircle (Q-tdTomato-IRES-hygro) forms were compared, it was clear that
225 minicircle donor vector mediated higher transposition efficiencies than the parental
226 plasmid form, irrespective of which helper plasmid was co-electroporated.
227 Moreover, cells co-electroporated with minicircle donor vector and helper plasmid
228 expressing *qPBase v2* consistently exhibited significantly higher transposition
229 activity than those receiving all other combinations, including those with the helper
230 plasmid expressing *hyPBase*. Based on these data in both Jurkat (Figure 3B) and
231 primary T cells (Figure 3C), we selected micro-*piggyBac* vector in the minicircle
232 DNA form as the donor vector and a series of recombinant *qPBase* (including

233 *qPBase v1* and *v2*) as the helper plasmids to form the *Quantum pBac*™ (*qPB*)
234 system (Figure 3D).

235 **When combined with CD20/CD19 CAR *Quantum pBac*™ (*qPB*) donor vector,**
236 ***Quantum PBase*™ (*qPBase v2*) outperforms *hyPBase* in CAR-T production**

237 We next evaluated the performance of CAR-T cells produced by
238 electroporating activated human primary T cells with vectors of the *qPB* system.

239 To do so, we used anti-CD20/CD19 CAR as the transgene cassette of *qPB* donor

240 vector and helper plasmids that encode either *hyPBase* or *qPBase v2*. (Figure 4A).

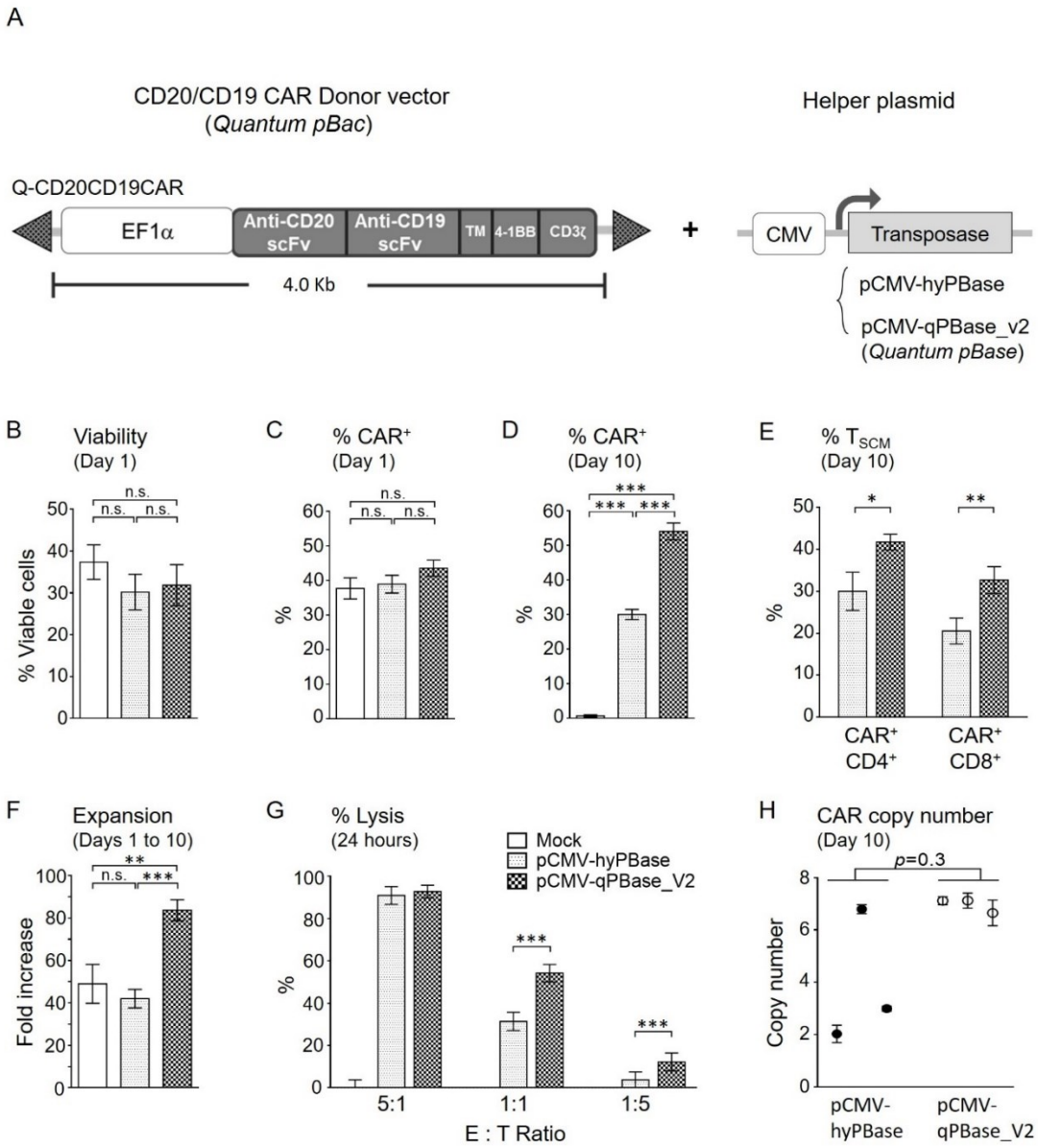

241

242

243 **Figure 4. CAR-T cell production using *Quantum pBac*™ (*qPB*) donor vector and helper**

244 **plasmid**

245 (A) Schematic depicts the CD20/CD19 CAR *qPB* donor vector and helper plasmid pCMV-hyPBase

246 or pCMV-qPBase_v2. Characterization of (B) cell viabilities one day after electroporation (Day 1).

247 Percentages of CAR$^+$ cells on (C) day 1 and (D) day 10 following electroporation of activated

248 primary T cells. (E) The percentages of CD4 and CD8 CAR^+ T_{SCM} cells on day 10. (F) Fold
249 expansion of cells after 10 days of culture, (G) cytotoxicity of day 10 CAR-T cells on Raji target
250 cells at the indicated E:T ratios, and (H) CAR copy number after 10 days of culture. Results are
251 shown as mean ± SD (B-H). n.s., p=0.3 not statistically significant, * $p < 0.05$, ** $p < 0.01$, *** $p <$
252 0.001. N = 3 (triplicate) except in (H) where testing of each sample was repeated three times per
253 sample.
254
255 One day after electroporation, no significant differences in viability or %
256 CAR^+ were found among cells electroporated with CD20/CD19 CAR *qPB* donor
257 vector and control helper plasmid (pCDNA3.1, Mock control) and those with helper
258 plasmid expressing either *hyPBase* or *qPBase v2* (Figure 4B, 4C). Notably, after
259 10 days of culture, significantly more CAR^+ cells were observed in cultures
260 electroporated with CD20/CD19 CAR *qPB* donor vector and helper plasmid
261 expressing *qPBase v2* compared to *hyPBase* (Figure 4D). Moreover, the
262 expansion and cytotoxic effects of cells electroporated with CD20/CD19 CAR *qPB*
263 donor vector and helper plasmid expressing *qPBase v2* were also significantly
264 greater than those seen in the other two groups of cells (Figure 4F and 4G). The
265 CAR copy numbers between *hyPBase*- and *qPBase v2*-transposed cells were not
266 significantly different (Figure 4H), even when CAR copy number is calculated to
267 reflect only CAR^+ cells (data not shown). These observations suggest that cells
268 electroporated with helper plasmid expressing *qPBase v2* were superior with

269 regards to their transposition efficiency, expansion capacity and anti-tumor
270 potency than cells electroporated with *hyPBase*-expressing plasmids.

271 ***Quantum PBase*™ produces CAR$^+$ T cells that are more highly enriched with**
272 **T_{SCM} subset than those produced by *hyPBase***

273 Since T_{SCM} enrichment is recognized as an important potential indicator of
274 clinical efficacy, we also compared the percentage of T_{SCM} in cells electroporated
275 with CD20/CD19 CAR *qPB* donor vector and helper plasmid expressing either
276 *hyPBase* or *qPBase v2* (Figure 4E). We found that in both CD4 and CD8
277 populations, the percentages of T_{SCM} cells were higher in cells electroporated with
278 helper plasmid expressing *qPBase v2* than *hyPBase.* Next, we focused on the
279 *qPB* system (*qPB* donor vector with *qPBase v2* helper plasmid) and sought to
280 determine whether there may be donor-dependent variations in CAR$^+$ cell
281 production using this system. We analyzed the performance of CAR-T cells

282 derived from peripheral blood mononuclear cells (PBMCs) of six healthy donors

283 (Figure 5).

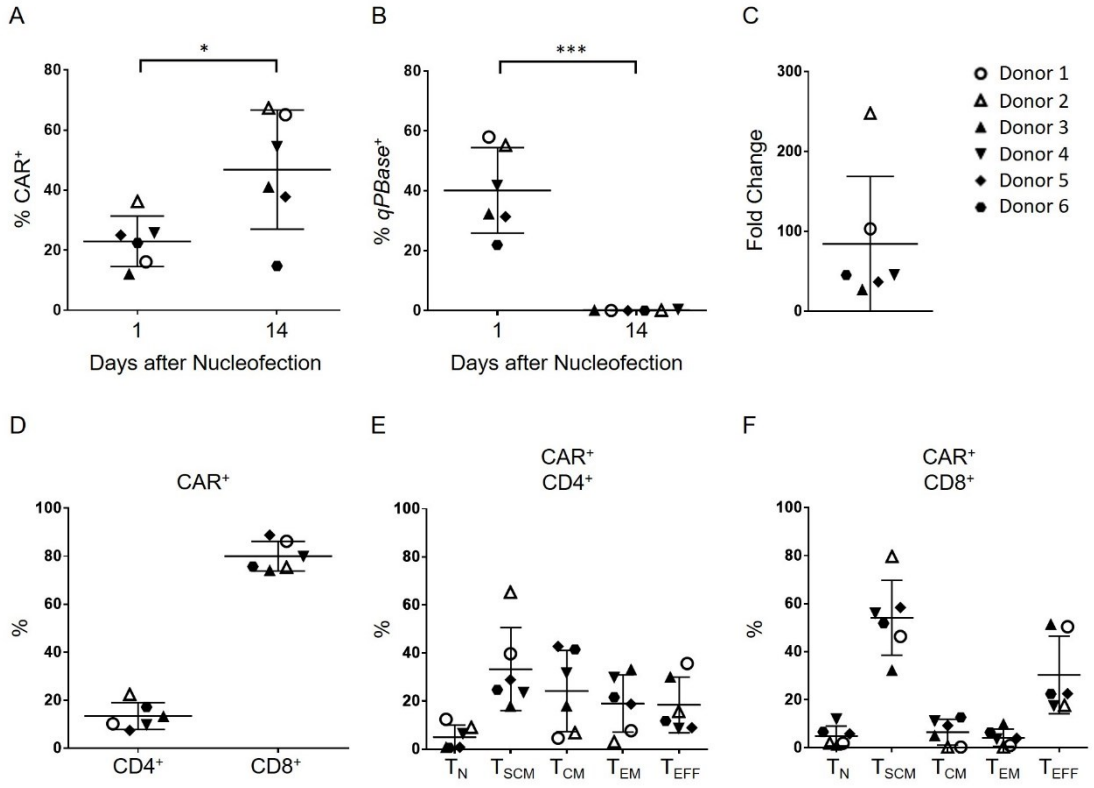

284

285 **Figure 5. Characterization of healthy donor CAR-T cells produced using the *Quantum***

286 ***pBac*™ (*qPB*) system**

287 Percentages of (A) CAR⁺ and (B) transposase⁺ (*qPBase*⁺) cells on days 1 and 14 following

288 electroporation. (C) Fold expansion of cells and (D) distributions of CD4⁺ and CD8⁺ T cell subtypes

289 in CAR⁺ T cells after 14 days of culture. Distributions of five T cell differentiation subsets T_N, T_{SCM},

290 T_{CM}, T_{EM} and T_{EFF} among (E) CD4⁺ CAR⁺ and (F) CD8⁺ CAR⁺ T cells on day 14. Results were

291 derived from cells taken from six healthy donors. Horizontal lines in (A-F) represent mean ± SD. *

292 $p < 0.05$, *** $p < 0.001$. N = 6 PMBC donors.

293

294 As shown in Figure 5A, the average percentage of CAR⁺ T cells significantly

295 increased from day 1 to 14 following electroporation, with only one of six donors

296 (donor 6) exhibiting a decrease in percentage of CAR$^+$ T cells. Moreover, fourteen
297 days after electroporation, the percentage of *qPBase*$^+$ cells decreased to minimal
298 levels (< 0.4%) in all of the donor groups (Figure 5B), suggesting successful
299 clearance of unwanted helper plasmids from T cells following completion of "cut-
300 and-paste" gene integration. There was high variability among the PBMC donor
301 groups in terms of the extent of CAR$^+$ T cell expansion during the 14-day culture
302 period (27- to 248-fold; Figure 5C), indicating a donor-dependent effect on
303 expansion capacity of the cells. We also profiled the T cell subtypes (CD4$^+$ and
304 CD8$^+$; Figure 5D) and T cell subsets based on differentiation stages (Figure 5E,
305 5F) among the CAR$^+$ T cells derived from the PBMC donors. CD8$^+$ T cells
306 comprised the major T cell subtype population (Figure 5D), despite the known
307 higher prevalence of CD4$^+$ T cells in human PBMCs. To analyze this
308 phenomenon, we carried out a time-course experiment to determine CD8/CD4
309 ratios before and up to 14 days following electroporation (Supplemental Figure 1).
310 We categorized the time course into three stages: transient transfection (up to 5
311 days post-electroporation), stable transgene integration (after 5-7 days post-
312 electroporation with undetectable transient CAR expression, Figure 4D), and cell
313 expansion (10 and 14 days post-electroporation). As shown, the CD8 enrichment
314 appeared to occur at the transfection (Supplemental Figure 1A and 1C) and the
315 cell expansion stages (after seven days in culture), but not at the stable transgene

316 integration stage (Supplemental Figure 1B, 1C and 1D). Furthermore, the major
317 CAR$^+$ T cell subset was T_{SCM} for both CD4 and CD8 populations (Figure 5E, 5F).

318 **_Quantum pBac_™ (_qPB_) system produces functional CAR$^+$ T cells that kill**
319 **target cells _in vitro_**

320 We next sought to determine whether CAR-T cells generated using the *qPB*
321 system (*qPB* donor vector with *qPBase v2* helper plasmid) are functional *in vitro*.
322 We conducted *in vitro* cytotoxicity assays by co-incubating antigen-expressing

323 target cells with either non-transfected control Pan-T cells or CD20/CD19 dual-

324 targeting CAR-T cells (Figure 6).

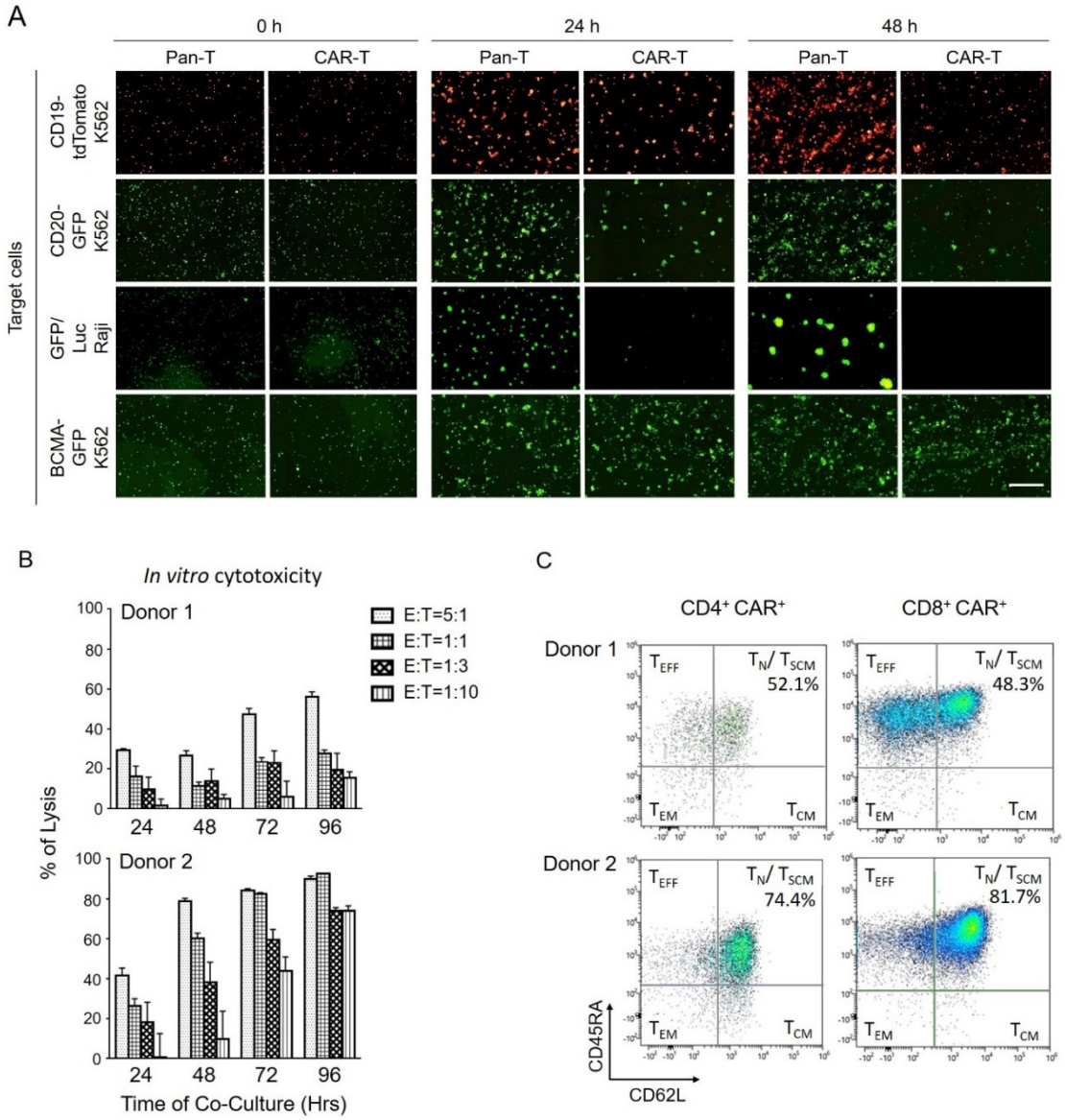

326

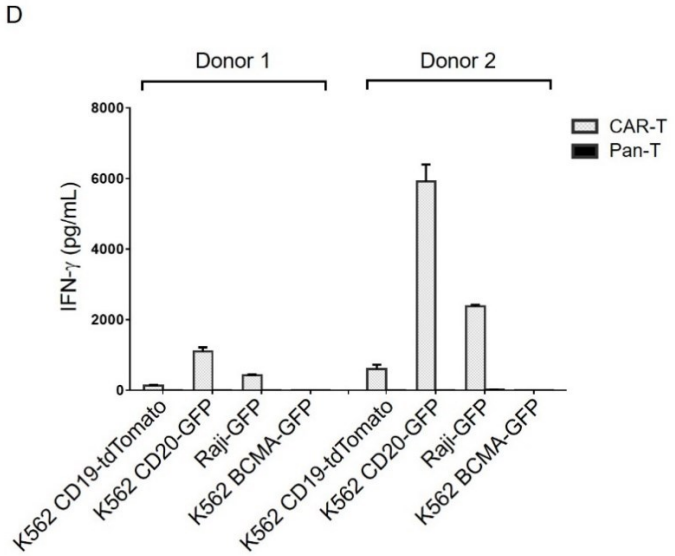

Figure 6. *In vitro* functional characterization of CAR-T cells produced using the *Quantum pBac*™ (*qPB*) system

In vitro cytotoxicity of Pan-T and/or CAR-T cells derived from healthy donor(s) (A) against the indicated target cells, and (B) against Raji cells at the indicated Effector: Target (E: T). (C) Representative flow cytometry data show the distributions of T cell differentiation subsets T_N/T_{SCM}, T_{CM}, T_{EM} and T_{EFF} in $CD4^+$ and $CD8^+$ subtypes for donor 1- and donor 2-derived CAR^+ T cells. (D) IFN-g secretion by donor 1 and donor 2 CAR-T cells following antigen stimulation. Pan-T cells (non-gene modified cells) served as a control. Data shown in (B and D) represent mean ± SD. N = 3 (triplicate). Bar in (A) represents 500 mm.

As shown in Figure 6A, compared to pan-T cells, CD20/CD19 dual-targeting CAR-T cells eradicated more $CD19^+CD20^+$ Raji cells (third row) and K562 target cells engineered to express either CD19 (first row) or CD20 (second row). On the other hand, CD20/CD19 dual-targeting CAR-T cells failed to eradicate BCMA (irrelevant antigen)-expressing control K562 cells (fourth row). These results demonstrated that the CAR-T cells specifically target and kill both CD20- and

344 CD19-expressing cells. The cytotoxic functions of CAR-T cells from two donors
345 (donors 1 and 2) were further assessed at different E:T ratios against Raji cells.
346 We observed dose- and time-dependent killing by CAR-T cells derived from both
347 donors (Figure 6B). Compared with donor 1-derived CAR-T cells, donor 2 CAR-T
348 cells were much more potent in killing Raji cells, which was consistent with the
349 relatively higher level of IFN-γ detected in the 48-hour culture medium of donor 2
350 CAR-T cells (Figure 6D). Notably, 74% of Raji cells were killed by donor 2 CAR-T
351 cells after a 96-h co-culture period even at a E:T ratio of 1:10 (Figure 6B). This
352 finding is in contrast to the 15.5% killing of Raji cells by donor 1 CAR-T cells at the
353 same E:T ratio. Together, these results suggest a higher level of persistence for
354 CAR-T cells derived from donor 2 as compared with those from donor 1.
355 Supporting this notion, the percentages of CAR^+ T_{SCM} cells were higher among
356 CAR-T cells from donor 2 (74.4% and 81.7% for $CD4^+$ and $CD8^+$ cells,
357 respectively) than those from donor 1 (52.1% and 48.3% for $CD4^+$ and $CD8^+$ cells,
358 respectively; Figure 6C).

359 **Effective tumor clearance by *Quantum pBac*™ (*qPB*)-generated CAR-T cells**
360 **in Raji-bearing immunodeficient mice**

361 Next, we tested the *in vivo* anti-tumor potency of donor 1 and donor 2 CAR-
362 T cells in Raji-bearing immunodeficient mice (Figure 7A). Similar to the *in vitro*
363 cytotoxicity results, injections of low, medium and high doses of donor 1 CAR-T
364 cells for five days killed Raji tumor cells in a dose-dependent fashion, and the

365 tumors were completely eradicated by Days 5 and 9 in mice injected respectively

366 with high and medium doses of donor 1 CAR-T cells (Figure 7B).

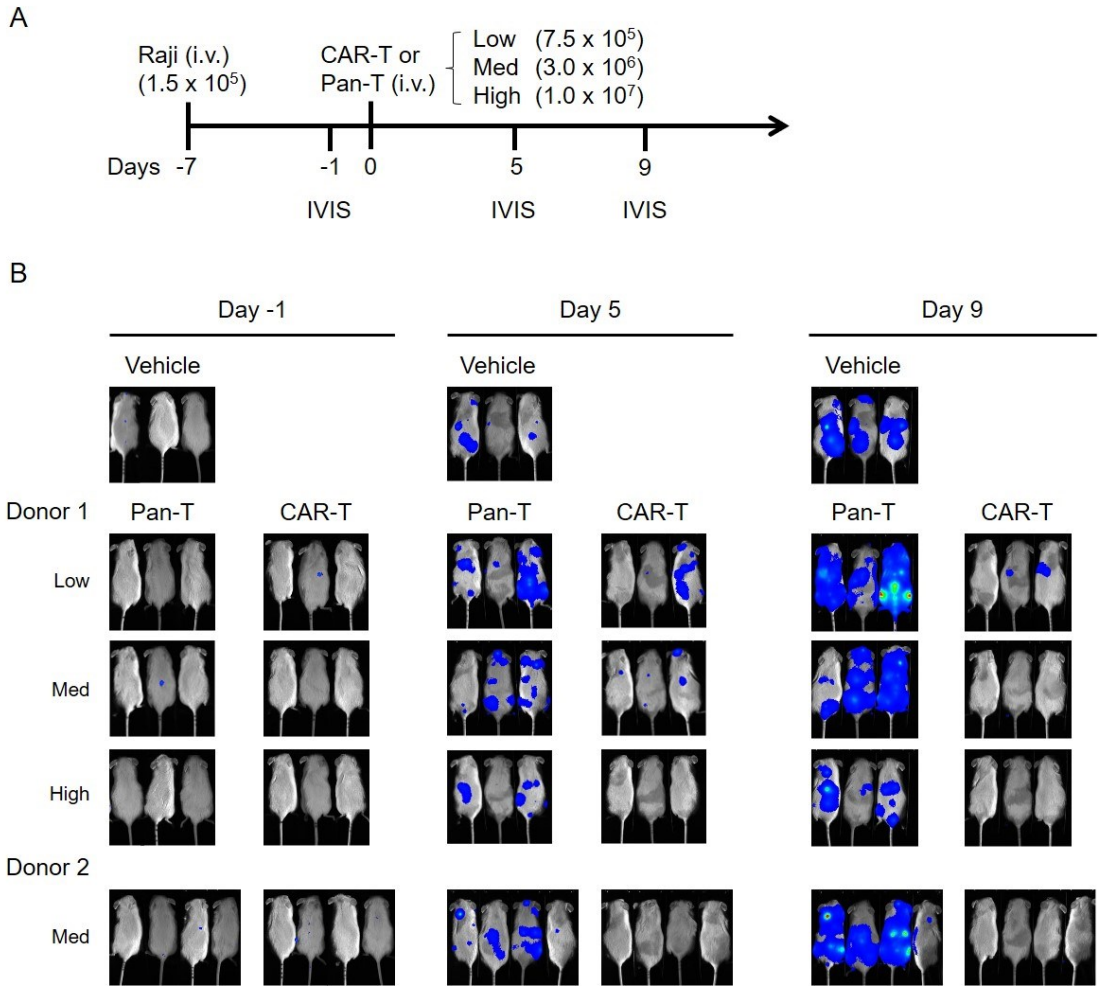

367

368

369 **Figure 7. *In vivo* functional characterization of CAR-T cells produced using the *Quantum***

370 ***pBac*™ (*qPB*) system in Raji-bearing immunodeficient mice**

371 (A) Schematic depicts the design of the *in vivo* functional characterization experiment. (B)

372 Bioluminescence imaging (IVIS) revealed the extent of tumor cell persistence 1 day prior to, and 5

373 and 9 days after CAR-T or Pan-T cell injection. N = 3 or 4 mice/group.

374

375 Consistent with these findings, a medium dose of donor 2 CAR-T cells also
376 eradicated Raji tumor cells from the Raji-bearing mice. Notably, the Raji tumor cell
377 killing by donor 2 CAR-T cells appeared to have occurred at an earlier time point
378 (at Day 5 following CAR-T cell injection) than that induced by donor 1 CAR-T cells
379 (at Day 9 following CAR-T cell injection) (Figure 7B), in agreement with the high *in*
380 *vitro* cytotoxicity induced by donor 2 CAR-T cells.
381

382 **Discussion**

383 *Sleeping Beauty* and *piggyBac* are two DNA transposons that have been
384 explored in recent clinical studies on gene and cell therapy[14,30]. In addition to the
385 multiple advantages over viral vectors mentioned earlier, the *piggyBac* transposon
386 system has at least four other major benefits. (1) It has a large cargo capacity (>
387 100 kb)[31]. (2) There is a low frequency of footprint-induced mutations caused by
388 integrant remobilization[32–34]. (3) *piggyBac* is perhaps the most active transposon
389 system in human cells[35]. (4) It is the most flexible transposon system in terms of
390 retained activity upon molecular engineering of the transposase; this aspect may
391 be crucial for applications that require modifications of the transposase to direct
392 site-specific *piggyBac* genomic integration. These unique features also make
393 *piggyBac* superior to *Sleeping Beauty* as a gene therapy vector. Nevertheless,
394 *Sleeping Beauty* is thought to be less genotoxic than *piggyBac* for two main
395 reasons: First, *piggyBac*-like terminal repeat elements are prevalent in the human
396 genome[36]. Second, unlike the far more random genome integration profile of
397 *Sleeping Beauty*, the genome integration profile of *piggyBac* is associated with

398 euchromatin and largely excluded from heterochromatin[37,38]. The relatively high
399 likelihood of *piggyBac* integration proximate to or within genes raises safety
400 concerns, since enhancer elements of retroviral vector long terminal repeats (LTR)
401 have previously been implicated as triggers of insertional mutagenesis in SCID-X1
402 patients[39].

403 The first above mentioned safety concern of *piggyBac* system was
404 thoroughly evaluated in a previous study,[40] which demonstrated that the
405 expression of transposase did not result in mobilization of endogenous *piggyBac*-
406 like sequences from the human genome[40]. The authors also did not find a
407 significant increase in double-stranded DNA breaks or a selective growth
408 advantage in *piggyBac*-harboring cells within long-term cultures of primary human
409 cells that were modified with eGFP-transposons[40]. To address the second above
410 mentioned concern (related to the potential risk of insertional mutagenesis
411 resulting from integrant enhancer activity), we determined whether enhancer
412 activity was present in the TRDs and/or the TIRs. We discovered that the IDS
413 region of 3' TRD contained significant enhancer activity (Figure 1). By removing
414 the IDS, our micro-*piggyBac* is expected to exhibit significantly lower levels of
415 enhancer activity, which in turn may improve the safety profile of the donor vector.
416 However, it has been well documented that both TIRs and other sequences
417 contained within the TRDs are crucial for efficient integration of *piggyBac*
418 transposon into the host genome. Several attempts to decrease the potential
419 genotoxicity by reducing the size of the required TRDs to approximately 100 base
420 pairs of TIRs have resulted in significant losses in transposition efficiency[27,41–43].

421 In contrast to these findings, our previous study[25] and the present study both
422 demonstrated that by deleting IDS from both ends and leaving only TIRs (107 bp
423 total in size), the transposition efficiency of *piggyBac* was in fact increased in
424 several instances (Figure 2 and Figure 3).[25]

425 Importantly, a significant increase in transposition efficiency was observed
426 in all cell types in which cells were co-transfected with a helper plasmid expressing
427 *qPBase v2* when compared to those transfected with plasmid expressing wild type
428 *PBase*. This finding suggests that *qPBase v2* is a robust and cell type-independent
429 *piggyBac* transposase that can exhibit high transposition activity irrespective of the
430 type and configuration of the *piggyBac* donor vector. We also demonstrated that
431 *qPBase v2* mediated significantly higher transposition activities than *hyPBase*
432 (1.8-fold increase in percentage of CAR^+ cells on day 10 over *hyPBase*; Figure
433 4D), while their CAR gene copy numbers did not significantly differ. Our previous
434 study has shown in a HEK293 genome-wide analysis of *qPBase v2*'s integration
435 sites that *qPBase v2* displayed a much more random integration profile with no
436 detectable hot spots, and has a lower preference for CpG islands and cancer-
437 related genes than *qPBase v1* or wild-type *PBase*.[26] Therefore, *qPBase v2*'s
438 enhanced transposition activities over *hyPBase* may be due to an increased
439 preference of *qPBase v2* for regions of the chromosome which promotes
440 transgene expression. With regards to the potential reason why cells produced
441 using *qPBase v2* expanded more than those produced using *hyPBase*, both the
442 above mentioned significantly higher transposition activities of *qPBase v2* as well
443 as the higher percentages of both CD4 and CD8 CAR^+ T_{SCM} (Figure 4D) likely play

444 a role. It is noteworthy that while the CAR copy numbers in our comparison
445 experiments seemed relatively high, we have determined in a separate study
446 related to manufacturing CAR-T cells for clinical applications that the total DNA
447 electroporated is positively-associated with CAR copy number in CAR-T cells. We
448 have subsequently optimized the donor:helper ratios to maximize generation of
449 CAR^+ T cells while maintaining acceptable CAR copy numbers.[44] Collectively, the
450 observations of this study suggest that micro-*piggyBac* in conjunction with *qPBase*
451 *v2* comprises a superior *piggyBac* system that outperforms other *piggyBac*
452 systems comprising *hyPBase*.

453 In addition to the impacts of TRDs/TIRs and transposase on the
454 performance of the *piggyBac* system, the method of introducing these components
455 into host cells can also greatly influence the transposition efficiency, potential
456 safety profile, and transgene stability of the *piggyBac* system. To ensure co-
457 transfection of both the transgene delivery cassette and the transposase gene, a
458 single plasmid transposon system was previously created wherein TRDs were
459 placed within the delivery cassette, and the transposase gene was located in the
460 helper part of the same plasmid[27]. However, such an arrangement had a few
461 disadvantages, including: (1) a reduced rate of gene delivery due to an increase in
462 size of DNA, a phenomenon particularly seen in electroporation-based gene
463 delivery, (2) a high degree of plasmid backbone DNA integration when using
464 transposon plasmids[27], and (3) a high rate of transposase gene integration into the
465 host genome[45]. For these reasons, we opted to utilize a two-component system,
466 consisting of donor vector and helper plasmid.

467 The use of a donor vector in plasmid form may have several undesirable
468 qualities for clinical translation, including the presence of bacterial genetic
469 elements and antibiotic-resistance genes. These features are undesirable since
470 they pose a significant safety risk if the plasmid backbone becomes transposed
471 into the host's genome. Additionally, unmethylated CpG motifs that are highly
472 enriched in the bacterial backbone of plasmids have been shown to trigger strong
473 inflammatory responses in host cells through toll-like receptor-9 associated
474 mechanisms. The sequences may also induce transgene silencing, presumably
475 via cellular immune responses[46] and/or interferon secretion[47].

476 To reduce the chance that such events may occur, a new *piggyBac* system
477 was established by incorporating *piggyBac* transposon into a doggybone™ DNA
478 (dbDNA) vector, which is a linear, covalently closed, minimal DNA vector produced
479 enzymatically *in vitro*[48]. A recent report has demonstrated that this *piggyBac*-
480 incorporated dbDNA can be used to generate stable CD19-targeting CAR-T cells
481 with an efficiency similar to that of its plasmid counterpart; the efficiencies were
482 comparable when a minimum of approximately 470 bp of additional randomly
483 selected DNA flanking the transposon was included. However, due to its linear
484 configuration, dbDNA is expected to be less efficient for electroporation-based
485 gene delivery as compared to its supercoiled circular counterpart. In this study,
486 we set out to increase *piggyBac*'s cargo capacity by using Mark Kay minicircle
487 technology to generate the smallest known *piggyBac* transposon donor vector with
488 TIRs (107 bp) and only 88 bp of the backbone sequence flanking the TIRs. The
489 small backbone sequence in combination with the truncated TRDs (i.e., TIRs) also

490 resulted in a marked decrease (more than 2 kb) in the size of the donor vector.
491 The smaller size donor vector in turn reduced DNA toxicity (i.e., electroporation-
492 induced cell damage) and enhanced the transfection rate, which respectively
493 improved cell expansion and transposition efficiency. This increase in
494 transposition efficiency was further amplified when the donor vector carried a
495 larger transgene (4.0 kb vs 5.34 kb). The end result of our modifications is that we
496 now have a *piggyBac* system that is capable of successfully delivering and
497 transposing larger size transgenes compared to *hyPB*. We demonstrated that use
498 of this transposon donor vector in conjunction with a highly active *qPBase v2*,
499 collectively designated as *Quantum pBac*™ (*qPB*), represents a superior *piggyBac*
500 system that is minimalistic, highly efficient, and potentially safe (Figure 3).

501 Currently, the failure rate for producing sufficient number of CAR^+ T cells
502 for therapy is quite high, and this high rate may be traced back to the scarcity of T
503 cells in some patients. Moreover, the T cells that remain in these patients are often
504 exhausted and senesced, making the cells more difficult to expand to reach clinical
505 quantity and quality criteria. In this study, we have addressed this obstacle with
506 our *qPB* system utilizing *qPBase v2*. This system can be utilized to effectively
507 generate CD19/CD20 dual-targeting CAR-T cells with a 1.8-fold increase in the
508 percentage of CAR^+ cells on day 10, and a 2-fold increase in the 10-day expansion
509 capacity, compared to *hyPBase* (Figure 4). Together, these increases in CAR-T
510 cell performance result in a 3.6-fold increase in the final yield of CAR-T cells. We
511 showed that this difference in yield is likely due to an enhanced transposition
512 efficiency achievable by the *qPB* system (Figure 3), and the increased yield should

513 facilitate the rapid generation of CAR^+ cells at a clinical scale. Likewise, the
514 significantly higher cytolytic activities of CAR-T cells produced using *qPBase v2*
515 compared with those produced using *hyPBase* (Figure 4G) likely reflect the
516 significantly higher percentage of CAR^+ cells in the cells produced by *qPBase v2*
517 than by *hyPBase* (Figure 4D) and greater proportion of T_{SCM} CAR^+ T cells (Figure
518 4E). This advance in technology may prevent the need to extend CAR-T cell
519 production time; such extensions may be required when using other CAR-T
520 production systems and may increase the risks of T cell exhaustion and
521 senescence that compromise CAR-T quality. The higher proportion of CAR^+ T cells
522 that are produced by using the *qPB* system should also allow for
523 injection/administration of fewer total cells, which may reduce the adverse effects
524 of CAR-T therapy. We have also shown that as the transgene size increased, the
525 percentage of CAR^+ cells decreased.[49] Since the difference in transposition
526 efficiencies between plasmid backbone-containing and plasmid backbone-lacking
527 donor vectors became more pronounced as transgene size increased (4.0 kb in
528 Figure 2D vs 5.34 kb in Figure 3C), we should be able to improve therapy results
529 by reducing the size of the donor vector to increase its capacity for therapeutic
530 transgene payload. Therefore, use of the *qPB* system, which is capable of carrying
531 a larger transgene cargo due to its reduced size, should enable the production of
532 efficacious CAR-T cells harboring sizable transgene(s) at a clinical scale.

533 It is noteworthy that there was a high representation of $CD8^+$ T cells in CAR^+
534 T cells produced using the *qPB* system (Figure 5D), despite the known high
535 prevalence of $CD4^+$ T cells in human PBMCs. As shown in Supplemental Figure

536 S1A, the CD8/CD4 ratio initially increased within one day post-electroporation,
537 suggesting that CD4 T cells may be more sensitive to electroporation-associated
538 damages. Subsequently, the further increase in CD8/CD4 ratio was positively
539 associated with a marked increase in cell expansion (see Figure S1C and S1B,
540 respectively), suggesting that the CD8 T cells were preferentially expanded
541 compared to the CD4 T cells. The fact that there was no change in CD8/CD4 ratio
542 at 5 and 7 days post-electroporation (when only transposed and not transfected
543 transgenes could be detected) also suggests that the pronounced enrichment of
544 CD8 T cells was not due to preferential transposition of CD8 T cells. As
545 demonstrated in another study, this preferential enrichment of CD8 T cells can
546 serve to complement the more difficult-to-enrich patient CD8 T cells and contribute
547 to a balanced CD8/CD4 ratio (approximately 1.0) in CAR-T cells produced from
548 patients with B-cell malignancies.[44]

549 Additionally, CAR-T cell expansion and persistence have emerged as key
550 efficacy determinants in cancer patients, and both are positively correlated with the
551 proportion of T_{SCM} cells in the final CAR-T cell product[50,51]. In line with these
552 findings, we have demonstrated that our *qPB*-derived CAR-T cells, which are
553 enriched in T_{SCM} cells (especially among $CD8^+$ CAR^+ T cells), exhibited potent anti-
554 tumor effects both *in vitro* and *in vivo*.

555 Another strategy to improve CAR-T therapy is to minimize genotoxicity caused
556 by transposase-induced integrant remobilization. To evaluate this potential
557 approach, transposase mRNA has been examined in transposon-based CAR-T
558 clinical trials[52]. However, compared to transposase DNA, the mRNA is generally

559 less efficient, more costly (for GMP production), and less stable under storage
560 conditions. Given the low frequency of footprint-induced mutation by *piggyBac*
561 (<5%) and the fact that only a minimal proportion (<0.4%) of CAR^+ T cells
562 expressed detectable levels of *qPBase* (Figure 5B), transposase in a plasmid form
563 should be sufficiently safe when applied to highly proliferative *ex vivo*-engineered
564 cells. Additionally, our recent genome-wide integration profiling of *qPB* in CAR-T
565 products derived from two distinct donors further support the notion that it is safe
566 to use in T cell engineering[49].

567 In summary, given its larger payload capacity compared to currently available
568 *piggyBac* systems and high level of efficiency, *qPB* is likely the most suitable
569 system for development of next generation virus-free gene and cell therapies,
570 especially for multiplex CAR-T therapy. As we have demonstrated in this study,
571 the *qPB* system exhibits greater transposition activity, causes less damage to cells,
572 induces a higher percentage of T_{SCM} and CAR^+ populations, and expands more of
573 the engineered cells than previous systems. These attributes lead to an overall
574 enhanced ability of the *qPB* system to produce highly CAR^+ T_{SCM} cells harboring
575 larger payloads, which should contribute to the success of *piggyBac*-based
576 multiplex CAR-T gene therapy. The success of *qPB* in CAR-T cell therapy
577 suggests that the technology may also be suitable for use in other gene therapy
578 applications as well.

579

580 **Materials and Methods**

581 **Human T cell samples from healthy donors**

582 Blood samples from adult healthy donors were obtained from Chang Gung
583 Memorial Hospital (Linkou, Taiwan). The acquisition of these samples was
584 approved by the Institution Review Board at Chang Gung Medical Foundation (IRB
585 No. 201900578A3).

586 **Vector constructs**

587 Plasmids were constructed following protocols described previously[53].
588 Minicircle DNAs were purchased from Aldevron (Fargo, ND). All of the PCR
589 products or junctions of constructs (wherever sequences were ligated) were
590 confirmed by sequencing.

591 ***Vector construction***

592 **pGL3-miniP (Construct a; Figure 1A)**

593 pGL3-basic was digested with SacI and HindIII. The CMV mini-promoter
594 with SacI and HindIII sequences on its 5' and 3' ends, respectively, was
595 synthesized, double-digested with SacI and HindIII, and ligated to the SacI-HindIII
596 vector fragment of pGL3-basic to make construct **a** as shown in Figure 1A.

597 **Constructs b-e (Figure 1A)**

598 pGL3-miniP was digested with KpnI and XhoI. The 5'TIR or 3'TIR of micro-
599 *piggyBac* or 5'TRD or 3'TRD of mini-*piggyBac* with KpnI and XhoI sequences
600 added on either end was synthesized, double-digested with KpnI and XhoI, and
601 ligated to the KpnI-XhoI vector fragment of pGL3-miniP, respectively, to make the
602 set of constructs (**b**-**e**) for evaluation of enhancer activity of mini-*piggyBac* and
603 micro-*piggyBac* TRDs and TIRs, respectively.

604

605 **Donor vectors (Figure 2A)**

606 "Mini-*piggyBac*-Long" was the same construct as the donor of *piggyBac*
607 system published previously [19]. "Micro-*piggyBac*-Short" was the plasmid named
608 "*pPB*-cassette short" in a previous publication[25]. "Micro-*piggyBac*-Long" was
609 constructed by replacing the backbone of "micro-*piggyBac*-Short" with that of "mini-
610 *piggyBac*-Long" via PCR-based cloning.

611 **Helper plasmid (Figure 2A)**

612 The construction of helper plasmid was described previously[26].

613 **Parental *qPB* donor vector (Figure 3A)**

614 The parental plasmid contained the following components (obtained by
615 DNA synthesis) arranged in a 5' to 3' order: Kanamycin resistance gene, origin of
616 replication (pMB1), 32 I-SceI sites, attB site (PhiC31), 5'TIR of micro-*piggyBac*,
617 multiple cloning site (MSC), 3'TIR of micro-*piggyBac*, and attP site (PhiC31).

618 **pQ-tdTomato-IRES-hygro (Figure 3A)**

619 The DNA for a cassette with the CAG promoter driving a bi-cistronic
620 transcript containing tdTomato gene, internal ribosome entry site (IRES) of Foot-
621 and-mouth disease virus (FMDV), and hygromycin resistance gene was
622 synthesized and cloned into the AseI and EcoRV sites of the parental *qPB* vector
623 to make pQ-tdTomato-IRES-hygro.

624 **pQ-CD20CD19CAR (Figure 4A)**

625 The dual-targeting tandem CD20/CD19 CAR-containing pQ-
626 CD20CD19CAR vector encoded a second-generation CAR composed of an
627 elongation factor 1-alpha (EF1α) promoter that drives an extracellular domain

628 derived from the single chain variable fragments (scFv) of monoclonal antibodies
629 directed against the CD19 and CD20 antigens, respectively. The sequence is
630 further linked to the CD3z chain of the TCR complex by means of a CD8 hinge and
631 transmembrane domains, together with the 4-1BB co-stimulatory domain.
632 Following synthesis, the expression cassette was cloned into the MCS of parental
633 *qPB* vector to make pQ-CD20CD19CAR.

634 **Minicircle DNA**

635 The minicircle DNAs, Q-tdTomato-IRES-hygro (Figure 3A) and Q-
636 CD20CD19CAR (Figure 4A), were manufactured by Aldevron from parental
637 plasmids, pQ-tdTomato-IRES-hygro and pQ-CD2019CAR, respectively.

638 ***qPBase***

639 To comply with the FDA regulations, the ampicillin gene in the helper
640 plasmid expressing *qPBase v2* was replaced by a kanamycin resistance gene
641 sequence to make *qPBase.* The *qPBase* component was combined with *qPB*
642 donor vector (minicircle DNA) to form the *qPB* system.

643 **Enhancer assay**

644 The control, pPL-TK (Renilla Luciferase), was co-transfected with the
645 specified firefly luciferase constructs (i.e., pGL3-miniP, pGL3-miniP-microL, pGL3-
646 miniP-microR, pGL3-miniP-miniR, pGL3-miniP-miniL, mini-*piggyBac* Long, micro-
647 *piggyBac* Short, or micro-*piggyBac* Long) by either FuGENE (HEK293) or
648 nucleofection (Sf9 cells, and Jurkat T cells). In some experiments, constructs were
649 first linearized using XmnI or BglI. Forty-eight hours after transfection, cells were

650 harvested and subjected to the Dual-Luciferase assay (Promega) according to the
651 manufacturer's instructions.

652 **Transposition assay**

653 HEK293 cells (1 x 10^5) were transfected with 200-334 ng of donor vector
654 carrying a hygromycin resistance gene and 200-282 ng of helper plasmid in MEM
655 medium (GeneDireX), 10% FBS (Corning) utilizing the X-tremeGENE™ HP DNA
656 transfection reagent (Merck). Transfected cells were transferred to 100-mm plates
657 and cultured under hygromycin (100 μg/ml) selection pressure for 14 days. Cells
658 were then harvested and fixed with 4% paraformaldehyde. Fixed cells were stained
659 with 0.2% methylene blue and cell colonies were counted.

660 Jurkat or primary T cells (2 x 10^5) were electroporated with 400-668 ng of
661 donor vector carrying a hygromycin resistance gene, which in some experiments
662 was also linked to a tdTomato gene, and 400-517 ng of helper plasmid in OpTmizer
663 medium supplemented with *Quantum Booster*™ (GenomeFrontier).
664 Electroporation was carried out using a 4D-Nucleofector™ (Lonza) in combination
665 with the *Quantum Nufect*™ Kit (GenomeFrontier) according to the manufacturer's
666 instructions. Electroporated cells were transferred to 96-well plates and cultured
667 under hygromycin (1 mg/ml) selection pressure for 14 days. Cells were then
668 harvested and stained with AO/PI. Live cell numbers were determined using Celigo
669 image cytometry (Nexcelom). Transposition efficiency was expressed as number
670 of either hygromycin-resistant colonies or live cells.

671

672

673 **Generation and expansion of CAR-T cells**

674 Peripheral blood mononuclear cells (PBMCs) were isolated from blood
675 samples of healthy donors by Ficoll-Hypaque gradient separation. $CD3^+$ T cells
676 were isolated from PBMCs using EasySep™ Human T Cell Isolation Kit (StemCell
677 Technologies) according to the manufacturer's instructions. T cells were activated
678 by co-incubation with anti-CD3/anti-CD28 antibody conjugated Dynabeads™
679 (Gibco, Catalogue No. 11141D) in X-VIVO 15 medium (Lonza) for two days at a
680 bead to cells ratio of 3:1. Following the removal of Dynabeads™, activated T cells
681 were harvested and frozen or utilized in experiments. Electroporation of activated
682 T cells was carried out using a Nucleofector™ 2b Device (Lonza) in combination
683 with the *Quantum Nufect*™ Kit (GenomeFrontier) according to the manufacturer's
684 instructions. Cells were electroporated with the combination of CD20/CD19 CAR
685 donor vector, and pCMV-hyPBase or pCMV-qPBase v2 helper vector. Cells were
686 cultured and expanded for 10 or 14 days in OpTmizer medium (Thermo Fisher
687 Scientific) supplemented with 50 IU of IL-2 (PeproTech) and 10% FBS. Thereafter,
688 the cells were harvested for experiments. γ-irradiated aAPCs were added on Day
689 3 to the T cell expansion cultures at an aAPC:T cell ratio of 1:1.

690 **Evaluation of CAR-T cells performance**

691 CAR expression on T cells was detected by flow cytometry following
692 staining of cells at 4°C for 30 min with $F(ab')_2$ fragment-specific, biotin-conjugated
693 goat anti-mouse antibodies (Jackson ImmunoResearch Laboratories) and R-
694 phycoerythrin (PE)-conjugated streptavidin (Jackson ImmunoResearch
695 Laboratories). Similarly, cells were stained with the following antigen-specific

696 fluorophore-conjugated antibodies: CD3-Pacific Blue, CD4-Alexa Flour 532
697 (Thermo Fisher Scientific), CD8-PE-Cy7, CD45RA-BV421, CD62L-PE-Cy5, or
698 CD95-BV711 (Biolegend). In some experiments, cells were incubated with
699 propidium iodide (PI, Thermo Fisher Scientific) and/or Acridine orange (AO,
700 Nexcelom). PI^- cells and T cell differentiation subsets were determined by flow
701 cytometry based on CD45RA, CD62L and CD95 expression, as follows: T_N
702 ($CD45RA^+CD62L^+CD95^-$), T_{SCM} ($CD45RA^+CD62L^+CD95^+$), T_{CM} ($CD45RA^-$
703 $CD62L^+$), T_{EM} ($CD45RA^-CD62L^-$), and T_{EFF} ($CD45RA^+CD62L^-$). *qPBase* expresses
704 a GFP-transposase fusion protein, which was detected by flow cytometry for GFP^+
705 cells. In some experiments, a hygromycin resistance gene was expressed with a
706 tdTomato gene and hygromycin-resistant cells were identified by flow cytometry
707 for $tdTomato^+$ cells. Flow cytometric measurements and analyses were performed
708 on a SA3800 Spectral Analyzer (Sony). Histograms and dot-plots were generated
709 using GraphPad Prism software (GraphPad). Live cells were detected using a
710 Celigo imaging cytometer (Nexcelom) as AO^+, PI^- cells.

711 ***In vitro* cytotoxicity assay**

712 Target-antigen-expressing cells were engineered according to a method
713 described elsewhere[49]. $CD19^+$ (K562 CD19-tdTomato), $CD20^+$ (K562 CD20-GFP),
714 $CD19^+CD20^+$ (Raji-GFP) or non-relevant K562 BCMA-GFP target cells were
715 seeded at 5 x 10^3 cells per well in 96-well culture plates (Corning), and control non-
716 transfected Pan-T or CAR-T cells were added at an E:T ratio of 5:1, 1:1, 1:3 or
717 1:10. Cytotoxicity of CAR-T cells on target cells was then assessed as previously
718 described[54]. Briefly, a Celigo imaging cytometer was used to measure the

719 percentage of live target cells at 0, 24, 48, 72 and 96 h of co-culture. Cell
720 aggregates were separated by pipetting prior to Celigo imaging. The percent of
721 specific lysis for each sample was calculated using the formula: [1-(live fluorescent
722 cell count in the presence of target cells and CAR-T cells / live fluorescent cell
723 count in the presence of target cells only)] x 100.

724 ***In vitro* cytokine release assay**

725 Pan-T control cells or CAR-T cells produced from two healthy donors were
726 thawed and added to cultures containing $CD19^+$ (K562 CD19-tdTomato), $CD20^+$
727 (K562 CD20-GFP), $CD19^+CD20^+$ (Raji-GFP) or non-relevant K562 BCMA-GFP
728 tumor target cells. The cells were added at an effector:target (E:T) ratio of 10:1 in
729 OpTmizer medium supplemented with 50 IU of IL-2 and 10% FBS. After 48 h of
730 co-culture, supernatant was collected and IFN-γ level in the culture supernatant
731 was measured by an enzyme-linked immunosorbent assay (Thermo Fisher),
732 according to the manufacturer's instructions.

733 **Mouse xenograft model**

734 *In vivo* studies on a mouse xenograft model were conducted at the
735 Development Center for Biotechnology, Taiwan, using animal protocols and
736 procedures ethically reviewed and approved by the Taiwan Mouse Clinic IACUC
737 (2020-R501-035). Briefly, 8-week-old female ASID (NOD.Cg-
738 $Prkdc^{scid}Il2rg^{tm1Wjl}$/YckNarl) mice (National Laboratory Animal Center, Taiwan)
739 were intravenously (i.v.) injected with 1.5 x 10^5 Raji-Luc/GFP tumor cells. One
740 week after Raji-Luc/GFP tumor cell injection, mice were injected with Low (7.5 x
741 10^5), Med (3 x 10^6), or High (1.0 x 10^7) doses of CAR-T cells or control Pan-T cells.

742 Luminescence signals from Raji-Luc/GFP tumor cells were monitored using the
743 Xenogen-IVIS Imaging System (Caliper Life Sciences).

744 **Statistical analysis**

745 Statistical analyses of differences between two groups were carried out
746 using Student's t-test (two-tail), and differences among three or more groups were
747 analyzed by one-way ANOVA with Tukey's multiple comparison test. The analyses
748 were performed using GraphPad Prism software (GraphPad Software), and
749 statistical significance was reported as * $p < 0.05$, ** $p < 0.01$, and *** $p < 0.001$.
750 Differences were considered to be statistically significant when $p < 0.05$.

751

752 **Acknowledgments**

753 The authors thank Ms. Lu-Chun Chen for her assistance throughout the IRB
754 preparation and approval process. The authors also thank Dr. Pei-Yi Tsai for
755 assistance with the animal experiments. This study was funded by
756 GenomeFrontier Therapeutics, Inc.

757

758 **Author Contributions:**

759 S.C.-Y.W. designed research. Y.-C.C. (Yi-Chun Chen), P.-N.W., Y.-S.Y.,
760 Y.-C.C. (Ying-Chun Chen), I.-C.C. performed research. W.-K.H., Y.-C.C. (Yi-Chun
761 Chen), J.C.H., K.-L.K.W., and S.C.-Y.W. analyzed data. J.C.H., P.S.C. and S.C.-
762 Y.W. wrote the paper.

763

764

765 **Declaration of Interests Statement:**

766 S.C.-Y.W. is the founder of GenomeFrontier Therapeutics, Inc., W.-K.H.,
767 Y.-C.C.(Yi-Chun Chen), K.-L.K.W., Y.-S.Y., Y.-C.C.(Ying-Chun Chen), I.-C.C., and
768 J.C.H. are affiliated with GenomeFrontier Therapeutics, Inc.

769

770 **Data Availability Statement**

771 The authors confirm that the data supporting the findings of this study are
772 available within the article and/or its supplementary materials.

773

774 **Keywords**

775 gene therapy | transposon | *piggyBac* | CAR-T

References

1. Ghosh, S., Brown, A.M., Jenkins, C., and Campbell, K. (2020). Viral Vector Systems for Gene Therapy: A Comprehensive Literature Review of Progress and Biosafety Challenges. Applied Biosafety *25*, 7–18. 10.1177/1535676019899502.

2. Nowrouzi, A., Glimm, H., von Kalle, C., and Schmidt, M. (2011). Retroviral vectors: Post entry events and genomic alterations. Viruses *3*, 429–455. 10.3390/v3050429.

3. Schröder, A.R.W., Shinn, P., Chen, H., Berry, C., Ecker, J.R., and Bushman, F. (2002). HIV-1 integration in the human genome favors active genes and local hotspots. Cell *110*, 521–529. 10.1016/S0092-8674(02)00864-4.

4. Cesana, D., Sgualdino, J., Rudilosso, L., Merella, S., Naldini, L., and Montini, E. (2012). Whole transcriptome characterization of aberrant splicing events induced by lentiviral vector integrations. Journal of Clinical Investigation *122*, 1667–1676. 10.1172/JCI62189.

5. Modlich, U., Navarro, S., Zychlinski, D., Maetzig, T., Knoess, S., Brugman, M.H., Schambach, A., Charrier, S., Galy, A., Thrasher, A.J., et al. (2009). Insertional transformation of hematopoietic cells by self-inactivating lentiviral and gammaretroviral vectors. Molecular Therapy *17*, 1919–1928. 10.1038/mt.2009.179.

6. Hacein-Bey-Abina, S., Garrigue, A., Wang, G.P., Soulier, J., Lim, A., Morillon, E., Clappier, E., Caccavelli, L., Delabesse, E., Beldjord, K., et al. (2008). Insertional oncogenesis in 4 patients after retrovirus-mediated gene therapy of SCID-X1. Journal of Clinical Investigation *118*, 3132–3142. 10.1172/JCI35700.

7. Cesana, D., Ranzani, M., Volpin, M., Bartholomae, C., Duros, C., Artus, A., Merella, S., Benedicenti, F., Sergi Sergi, L., Sanvito, F., et al. (2014). Uncovering and dissecting the genotoxicity of self-inactivating lentiviral vectors in vivo. Molecular Therapy *22*, 774–785. 10.1038/mt.2014.3.

8. Jähner, D., and Jaenisch, R. (1985). Retrovirus-induced de novo methylation of flanking host sequences correlates with gene inactivity. Nature *315*, 594–597. 10.1038/315594a0.

9. Jähner, D., Stuhlmann, H., Stewart, C.L., Harbers, K., Löhler, J., Simon, I., and Jaenisch, R. (1982). De novo methylation and expression of retroviral genomes during mouse embryogenesis. Nature *298*, 623–628. 10.1038/298623a0.

10. Raper, S.E., Chirmule, N., Lee, F.S., Wivel, N.A., Bagg, A., Gao, G.P., Wilson, J.M., and Batshaw, M.L. (2003). Fatal systemic inflammatory response syndrome in a ornithine transcarbamylase deficient patient following adenoviral gene transfer. Mol Genet Metab *80*, 148–158. 10.1016/j.ymgme.2003.08.016.

11. van der Loo, J.C.M., and Wright, J.F. (2016). Progress and challenges in viral vector manufacturing. Hum Mol Genet *25*, R42–R52. 10.1093/hmg/ddv451.

812 12. Ramamoorth, M., and Narvekar, A. (2015). Non viral vectors in gene therapy - An
813 overview. Journal of Clinical and Diagnostic Research *9*, GE01–GE06.
814 10.7860/JCDR/2015/10443.5394.

815 13. Meir, Y.J.J., and Wu, S.C.Y. (2011). Transposon-based vector systems for gene therapy
816 clinical Trials: Challenges and considerations. Chang Gung Med J *34*, 565–579.

817 14. Tipanee, J., Chai, Y.C., Driessche, T. vanden, and Chuah, M.K. (2017). Preclinical and
818 clinical advances in transposon-based gene therapy. Biosci Rep *37*, BSR20160614.
819 10.1042/BSR20160614.

820 15. Ivics, Z., Hackett, P.B., Plasterk, R.H., and Izsvák, Z. (1997). Molecular reconstruction of
821 sleeping beauty, a Tc1-like transposon from fish, and its transposition in human cells. Cell
822 *91*, 501–510. 10.1016/S0092-8674(00)80436-5.

823 16. Ivics, Z., and Izsvák, Z. (2005). A whole lotta jumpin' goin' on: New transposon tools for
824 vertebrate functional genomics. Trends in Genetics *21*, 8–11. 10.1016/j.tig.2004.11.008.

825 17. Fraser, M.J., Smith, G.E., and Summers, M.D. (1983). Acquisition of Host Cell DNA
826 Sequences by Baculoviruses: Relationship Between Host DNA Insertions and FP Mutants
827 of Autographa californica and Galleria mellonella Nuclear Polyhedrosis Viruses. J Virol *47*,
828 287–300. 10.1128/jvi.47.2.287-300.1983.

829 18. Ding, S., Wu, X., Li, G., Han, M., Zhuang, Y., and Xu, T. (2005). Efficient transposition of
830 the piggyBac (PB) transposon in mammalian cells and mice. Cell *122*, 473–483.
831 10.1016/j.cell.2005.07.013.

832 19. Wu, S.C.Y., Meir, Y.J.J., Coates, C.J., Handler, A.M., Pelczar, P., Moisyadi, S., and Kaminski,
833 J.M. (2006). piggyBac is a flexible and highly active transposon as compared to Sleeping
834 Beauty, Tol2, and Mos1 in mammalian cells. Proc Natl Acad Sci U S A *103*, 15008–15013.
835 10.1073/pnas.0606979103.

836 20. Mátés, L., Chuah, M.K.L., Belay, E., Jerchow, B., Manoj, N., Acosta-Sanchez, A., Grzela,
837 D.P., Schmitt, A., Becker, K., Matrai, J., et al. (2009). Molecular evolution of a novel
838 hyperactive Sleeping Beauty transposase enables robust stable gene transfer in
839 vertebrates. Nat Genet *41*, 753–761. 10.1038/ng.343.

840 21. Voigt, F., Wiedemann, L., Zuliani, C., Querques, I., Sebe, A., Mátés, L., Izsvák, Z., Ivics, Z.,
841 and Barabas, O. (2016). Sleeping Beauty transposase structure allows rational design of
842 hyperactive variants for genetic engineering. Nat Commun *7*, 11126.
843 10.1038/ncomms11126.

844 22. Cadiñanos, J., and Bradley, A. (2007). Generation of an inducible and optimized piggyBac
845 transposon system. Nucleic Acids Res *35*, e87. 10.1093/nar/gkm446.

846 23. Yusa, K., Zhou, L., Li, M.A., Bradley, A., and Craig, N.L. (2011). A hyperactive piggyBac
847 transposase for mammalian applications. Proc Natl Acad Sci U S A *108*, 1531–1536.
848 10.1073/pnas.1008322108.

849 24. Yusa, K. (2015). piggyBac transposon. In Mobile DNA III (ASM Press), pp. 873–890.
850 10.1128/9781555819217.ch39.

851 25. Meir, Y.J.J., Weirauch, M.T., Yang, H.S., Chung, P.C., Yu, R.K., and Wu, S.C.Y. (2011).
852 Genome-wide target profiling of piggyBac and Tol2 in HEK 293: Pros and cons for gene
853 discovery and gene therapy. BMC Biotechnol *11*, 28. 10.1186/1472-6750-11-28.

854 26. Meir, Y.J.J., Lin, A., Huang, M.F., Lin, J.R., Weirauch, M.T., Chou, H.C., Lin, S.J.A., and Wu,
855 S.C.Y. (2013). A versatile, highly efficient, and potentially safer piggyBac transposon
856 system for mammalian genome manipulations. FASEB Journal *27*, 4429–4443.
857 10.1096/fj.12-223586.

858 27. Solodushko, V., Bitko, V., and Fouty, B. (2014). Minimal piggyBac vectors for chromatin
859 integration. Gene Ther *21*, 1–9. 10.1038/gt.2013.52.

860 28. Cooney, A.L., Singh, B.K., and Sinn, P.L. (2015). Hybrid nonviral/viral vector systems for
861 improved piggyBac DNA transposon in vivo delivery. Molecular Therapy *23*, 667–674.
862 10.1038/mt.2014.254.

863 29. Kay, M.A., He, C.Y., and Chen, Z.Y. (2010). A robust system for production of minicircle
864 DNA vectors. Nat Biotechnol *28*, 1287–1289. 10.1038/nbt.1708.

865 30. Magnani, C.F., Tettamanti, S., Alberti, G., Pisani, I., Biondi, A., Serafini, M., and Gaipa, G.
866 (2020). Transposon-Based CAR T Cells in Acute Leukemias: Where are We Going? Cells *9*,
867 1337. 10.3390/cells9061337.

868 31. Li, R., Zhuang, Y., Han, M., Xu, T., and Wu, X. (2013). PiggyBac as a high-capacity
869 transgenesis and gene-therapy vector in human cells and mice. DMM Disease Models
870 and Mechanisms *6*, 828–833. 10.1242/dmm.010827.

871 32. Elick, T.A. (1996). Excision of the piggy Bac transposable element in vitro is a precise
872 event that is enhanced by the expression of its encoded transposase. Genetica *98*, 33–41.
873 10.1007/BF00120216.

874 33. Li, M.A., Pettitt, S.J., Eckert, S., Ning, Z., Rice, S., Cadiñanos, J., Yusa, K., Conte, N., and
875 Bradley, A. (2013). The piggyBac Transposon Displays Local and Distant Reintegration
876 Preferences and Can Cause Mutations at Noncanonical Integration Sites. Mol Cell Biol *33*,
877 1317–1330. 10.1128/mcb.00670-12.

878 34. Chen, Q., Luo, W., Veach, R.A., Hickman, A.B., Wilson, M.H., and Dyda, F. (2020).
879 Structural basis of seamless excision and specific targeting by piggyBac transposase. Nat
880 Commun *11*, 3446. 10.1038/s41467-020-17128-1.

881 35. Doherty, J.E., Huye, L.E., Yusa, K., Zhou, L., Craig, N.L., and Wilson, M.H. (2012).
882 Hyperactive piggybac gene transfer in human cells and in vivo. Hum Gene Ther *23*, 311–
883 320. 10.1089/hum.2011.138.

884 36. Feschotte, C. (2006). The piggyBac transposon holds promise for human gene therapy.
885 Proc Natl Acad Sci U S A *103*, 14981–14982. 10.1073/pnas.0607282103.

886 37. Galvan, D.L., Nakazawa, Y., Kaja, A., Kettlun, C., Cooper, L.J.N., Rooney, C.M., and Wilson,
887 M.H. (2009). Genome-wide mapping of piggybac transposon integrations in primary
888 human T cells. Journal of Immunotherapy *32*, 837–844. 10.1097/CJI.0b013e3181b2914c.

889 38. Hamada, M., Nishio, N., Okuno, Y., Suzuki, S., Kawashima, N., Muramatsu, H., Tsubota, S.,
890 Wilson, M.H., Morita, D., Kataoka, S., et al. (2018). Integration Mapping of piggyBac-
891 Mediated CD19 Chimeric Antigen Receptor T Cells Analyzed by Novel Tagmentation-
892 Assisted PCR. EBioMedicine *34*, 18–26. 10.1016/j.ebiom.2018.07.008.

893 39. Hacein-Bey-Abina, S., von Kalle, C., Schmidt, M., McCormack, M.P., Wulffraat, N.,
894 Leboulch, P., Lim, A., Osborne, C.S., Pawliuk, R., Morillon, E., et al. (2003). LMO2-
895 Associated Clonal T Cell Proliferation in Two Patients after Gene Therapy for SCID-X1.
896 Science (1979) *302*, 415–419. 10.1126/science.1088547.

897 40. Saha, S., Woodard, L.E., Charron, E.M., Welch, R.C., Rooney, C.M., and Wilson, M.H.
898 (2015). Evaluating the potential for undesired genomic effects of the piggyBac
899 transposon system in human cells. Nucleic Acids Res *43*, 1770–1782.
900 10.1093/nar/gkv017.

901 41. Li, X., Harrell, R.A., Handler, A.M., Beam, T., Hennessy, K., and Fraser, M.J. (2005).
902 piggyBac internal sequences are necessary for efficient transformation of target
903 genomes. Insect Mol Biol *14*, 17–30. 10.1111/j.1365-2583.2004.00525.x.

904 42. Elick, T.A., Lobo, N., and Fraser, M.J. (1997). Analysis of the cis-acting DNA elements
905 required for piggyBac transposable element excision. Molecular and General Genetics
906 *255*, 605–610. 10.1007/s004380050534.

907 43. Li, X., Lobo, N., Bauser, C.A., and Fraser, M.J. (2001). The minimum internal and external
908 sequence requirements for transposition of the eukaryotic transformation vector
909 piggyBac. Molecular Genetics and Genomics *266*, 190–198. 10.1007/s004380100525.

910 44. Chang, P.S., Chen, Y.-C., Hua, W.-K., Hsu, J.C., Tsai, J.-C., Huang, Y.-W., Kao, Y.-H., Wu, P.-
911 H., Chang, Y.-F., Chang, M.-C., et al. (2022). Manufacturing highly potent CD20/CD19-
912 targeted iCasp9 regulatable CAR-T cells using the Quantum pBac-based CAR-T (qCART)
913 system for clinical application. bioRxiv. https://doi.org/10.1101/2022.05.03.490475.

914 45. Urschitz, J., Kawasumi, M., Owens, J., Morozumi, K., Yamashiro, H., Stoytchev, I., Marh, J.,
915 Dee, J.A., Kawamoto, K., Coates, C.J., et al. (2010). Helper-independent piggyBac plasmids
916 for gene delivery approaches: Strategies for avoiding potential genotoxic effects. Proc
917 Natl Acad Sci U S A *107*, 8117–8122. 10.1073/pnas.1003674107.

918 46. Chen, Z.Y., Yant, S.R., He, C.Y., Meuse, L., Shen, S., and Kay, M.A. (2001). Linear DNAs
919 concatemerize in vivo and result in sustained transgene expression in mouse liver.
920 Molecular Therapy *3*, 403–410. 10.1006/mthe.2001.0278.

921 47. Huerfano, S., Ryabchenko, B., and Forstová, J. (2013). Nucleofection of expression
922 vectors induces a robust interferon response and inhibition of cell proliferation. DNA Cell
923 Biol *32*, 467–479. 10.1089/dna.2012.1950.

924 48. Bishop, D.C., Caproni, L., Gowrishankar, K., Legiewicz, M., Karbowniczek, K., Tite, J.,
925 Gottlieb, D.J., and Micklethwaite, K.P. (2020). CAR T Cell Generation by piggyBac
926 Transposition from Linear Doggybone DNA Vectors Requires Transposon DNA-Flanking
927 Regions. Mol Ther Methods Clin Dev *17*, 359–368. 10.1016/j.omtm.2019.12.020.

928 49. Chen, Y.-C., Hua, W.-K., Hsu, J.C., Chang, P.S., Wen, K.K.-L., Huang, Y.-W., Tsai, J.-C., Kao,
929 Y.-H., Wu, P.-H., Wang, P.-N., et al. (2022). Quantum CART (qCART), a piggyBac-based
930 system for development and production of virus-free multiplex CAR-T cell therapy.
931 bioRxiv. 10.1101/2022.05.03.490469.

932 50. Gattinoni, L., Speiser, D.E., Lichterfeld, M., and Bonini, C. (2017). T memory stem cells in
933 health and disease. Nat Med *23*, 18–27. 10.1038/nm.4241.

934 51. Biasco, L., Izotova, N., Rivat, C., Ghorashian, S., Richardson, R., Guvenel, A., Hough, R.,
935 Wynn, R., Popova, B., Lopes, A., et al. (2021). Clonal expansion of T memory stem cells
936 determines early anti-leukemic responses and long-term CAR T cell persistence in
937 patients. Nat Cancer *2*, 629–642. 10.1038/s43018-021-00207-7.

938 52. Prommersberger, S., Reiser, M., Beckmann, J., Danhof, S., Amberger, M., Quade-Lyssy, P.,
939 Einsele, H., Hudecek, M., Bonig, H., and Ivics, Z. (2021). CARAMBA: a first-in-human
940 clinical trial with SLAMF7 CAR-T cells prepared by virus-free Sleeping Beauty gene
941 transfer to treat multiple myeloma. Gene Ther *28*, 560–571. 10.1038/s41434-021-00254-
942 w.

943 53. Sambrook, J., and Russell, D.W. (2001). Molecular Cloning: A Laboratory Manual, Third
944 Edition. In Molecular Cloning: a laboratory a manual, pp. 1.32-1.34.

945 54. Sun, Y.-J., Chen, Y.-C., Hua, W.-K., Wu, S.C.-Y., and Chan, L. (2022). Comparison of
946 chimeric antigen receptor-T cell-mediated cytotoxicity assays with suspension tumor
947 cells using plate-based image cytometry method. Cytometry A. 10.1002/cyto.a.24673.

948